



# Linking global terrestrial CO<sub>2</sub> fluxes and environmental drivers using OCO-2 and a geostatistical inverse model

Zichong Chen<sup>1</sup>, Junjie Liu<sup>2</sup>, Daven K. Henze<sup>3</sup>, Deborah N. Huntzinger<sup>4</sup>, Kelley C. Wells<sup>5</sup>, and Scot M. Miller<sup>1</sup>

<sup>1</sup>Department of Environmental Health and Engineering, Johns Hopkins University, Baltimore, MD, USA

<sup>2</sup>Jet Propulsion Laboratory, California Institute of Technology, Pasadena, CA, USA

<sup>3</sup>Department of Mechanical Engineering, University of Colorado Boulder, Boulder, CO, USA

<sup>4</sup>School of Earth and Sustainability, Northern Arizona University, Flagstaff, AZ, USA

<sup>5</sup>Department of Soil, Water, and Climate, University of Minnesota-Twin Cities, St. Paul, MN, USA

**Correspondence:** Zichong Chen (zchen74@jhu.edu)

**Abstract.** Observations from the Orbiting Carbon Observatory 2 (OCO-2) satellite, launched in July 2014, have been used to estimate CO<sub>2</sub> fluxes in many regions of the globe and provide new insight on the global carbon cycle. A challenge now is to not only estimate fluxes using satellite observations but also to understand how these fluxes are connected to variations in environmental conditions. In this study, we specifically evaluate the capabilities and limitations of utilizing current OCO-2 observations to infer connections between CO<sub>2</sub> fluxes and underlying environmental variables. To do so, we adapt geostatistical inverse modeling to satellite-based applications and evaluate a case study for year 2016 using OCO-2. A unique aspect of the geostatistical approach is that we can use estimates of environmental and meteorological variables to help estimate CO<sub>2</sub> fluxes in place of a traditional prior flux model. We are able to quantify the relationships between CO<sub>2</sub> fluxes and a few environmental variables across global biomes; we find that a simple combination of air temperature, daily precipitation, and photosynthetically active radiation (PAR) can describe almost 90% of the variability in CO<sub>2</sub> fluxes as seen through OCO-2 observations. PAR is an adept predictor of fluxes across mid-to-high latitudes, whereas a combined set of air temperature and precipitation shows strong explanatory power across tropical biomes. However, we are unable to quantify relationships with additional environmental variables because many variables are correlated or colinear when passed through an atmospheric model and averaged across a total atmospheric column. Overall, we estimate a global net biospheric flux of  $-1.73 \pm 0.53$  GtC in year 2016, in close agreement with recent inverse modeling studies using OCO-2 retrievals as observational constraints.

## 1 Introduction

Over the past decade, the field of space-based CO<sub>2</sub> monitoring has undergone a rapid evolution. The sheer number of CO<sub>2</sub>-observing satellites has greatly increased, including GOSAT/GOSAT-2 (Kuze et al., 2009; Nakajima et al, 2012), TanSat (Yang et al., 2018) and OCO-2/OCO-3 (Crisp, 2015; Eldering et al., 2019). These dramatically expanded satellites observe atmospheric CO<sub>2</sub> broadly across the globe, making it possible to estimate the distribution and magnitude of CO<sub>2</sub> fluxes in many regions of the globe that previously had sparse *in situ* surface atmospheric CO<sub>2</sub> monitoring (e.g., the tropics and the



Southern Hemisphere). For example, the OCO-2 satellite, launched in July 2014, provides 65,000 high-quality observations per day (Eldering et al., 2017); the dense, global set of OCO-2 observations, combined with inverse modeling techniques, have been used to constrain regional- and continental-scale CO<sub>2</sub> sources and sinks and provide new insights into CO<sub>2</sub> fluxes (e.g., Liu et al., 2017; Crowell et al. 2019; Palmer et al., 2019).

Furthermore, recent advances in OCO-2 retrievals from the NASA ACOS science team have led to widespread improvements in the observations (e.g., O'Dell et al., 2018), and these improvements have enabled increasingly accurate and detailed CO<sub>2</sub> flux constraints from inverse modeling (e.g., Miller and Michalak, 2020). Reducing the biases in satellite retrievals is critical for understanding CO<sub>2</sub> sources and sinks using inverse modeling, as even small retrieval biases can have a large impact on the CO<sub>2</sub> flux estimate (e.g., Chevallier et al, 2014; Miller et al., 2018). For example, Miller et al (2018) evaluated the extent to which OCO-2 retrievals can detect patterns in biospheric CO<sub>2</sub> fluxes and found that an early version of the OCO-2 retrievals (version 7) is only equipped to provide accurate flux constraints across very large continental or hemispheric regions; by contrast, in a companion paper, Miller and Michalak (2020) re-visited satellite capabilities in light of recently improved OCO-2 retrievals, and the authors suggested that new OCO-2 retrievals can be used to constrain CO<sub>2</sub> fluxes for more detailed regions (i.e., for seven global biomes).

A challenge now is to not only estimate the magnitude and distribution of fluxes using these new OCO-2 retrievals but also to understand how variations in fluxes are connected to variations in environmental drivers. We define the term “environmental drivers” as any meteorological variables or characteristics of the physical environment that can be modeled or measured and may correlate with net ecosystem exchange (NEE). Existing studies on the capability of satellite observations have widely focused on constraining the magnitude and distribution of fluxes (e.g., Eldering et al., 2017; Liu et al., 2017; Palmer et al., 2019; Crowell et al., 2019; Chevallier et al., 2019). It is now time to push these satellite observations further and explore whether the observations can be used to infer connections between fluxes and environmental drivers (refer to hereafter as ‘connections’) across many different regions of the globe. Variations in CO<sub>2</sub> fluxes are closely linked with variations in environmental drivers, and understanding these connections is key if we are to use these new satellite observations to evaluate and improve process-based terrestrial biospheric models (TBMs).

These connections have been extensively studied at local and global scales. At site levels (~1 km<sup>2</sup>), eddy covariance flux tower measurements have provided excellent detail to quantify these connections (e.g., Desai et al., 2010; Baldocchi et al., 2017); At the global level, existing studies (e.g, Wang et al., 2014; Keppel-Aleks et al., 2014; Piao et al., 2013) used atmospheric CO<sub>2</sub> from global background stations (e.g., Mauna Loa, Hawaii, USA and the South Pole) to illustrate a global picture of these connections. However, intermediate, regional-scale connections are still poorly understood (e.g., Niu et al., 2017; Shiga et al., 2018). To date, previous studies have used ground-based and aircraft observations of atmospheric CO<sub>2</sub> to link the fluxes and underlying environmental processes (e.g., Gourdji et al., 2012; Fang and Michalak, 2015; Fang et al., 2017; Shiga et al., 2018; Hu et al., 2019). However, it is difficult to constrain these connections for regions with few *in situ* atmospheric CO<sub>2</sub> observations (e.g., the tropics and the Southern Hemisphere). The global coverage of OCO-2 observations provides a novel opportunity to bridge the gap and explore these connections on region scales (e.g., Eldering et al., 2017; Liu et al. 2017).



However, it is still unclear the extent to which we can make these regional-scale connections given the accuracy and coverage of current OCO-2 observations. Indeed, Liu et al. (2017) used net biosphere fluxes inferred from version seven OCO-2 retrievals along with component carbon fluxes to disentangle environmental processes related to the flux anomalies in tropical regions during the 2015-2016 El Niño. However, Chevallier (2018) suggested that the satellite retrievals used in Liu et al (2017) cannot provide sufficient accuracy and sensitivity to separately constrain continental flux anomalies and associated environmental processes over the tropics. Hence, we specifically evaluate the capability and limitation of using current OCO-2 retrievals to infer these connections on regional scales using a geostatistical inverse modeling (GIM).

A GIM is particularly well-suited to systematically evaluating these connections. Specifically, a GIM does not prescribe or rely on a traditional prior flux model. The choice of prior fluxes in a classical inverse model is often subjective, and this choice can impact the posterior flux estimate (e.g., Peylin et al., 2013; Houweling et al., 2015; Philip et al., 2019). By contrast, a GIM can assimilate a wide range of environmental drivers, making it possible to evaluate data-driven connections between these variations in environmental drivers and CO<sub>2</sub> fluxes inferred from atmospheric observations (see Sect. 2). Existing GIM studies have investigated connections of CO<sub>2</sub> fluxes and environmental drivers for North America (Gourdji et al., 2010, 2012; Commane et al., 2017; Shiga et al. 2018) and the globe (Gourdji et al., 2008) using a variety of *in situ* CO<sub>2</sub> observations.

GIMs, however, have never been applied to global satellite observations, and the extension of GIMs from small, regional *in situ* datasets to a massive, global satellite datasets like OCO-2 presents novel computational and statistical challenges. To overcome this challenge, we combine the GIM with the adjoint of a global chemical transport model. Using this framework, we not only estimate daily global CO<sub>2</sub> fluxes at the model grid scale (4° latitude × 5° longitude) but also quantify posterior uncertainties in the estimated fluxes. This study builds upon previous efforts (Miller et al., 2018; Miller and Michalak, 2020) in which the authors evaluated when and where the OCO-2 observations can be used to constrain biospheric CO<sub>2</sub> fluxes. In this study we push one step further and explore the connections between CO<sub>2</sub> fluxes and environmental drivers. The primary purpose of this study is to couple a GIM to a global adjoint model and use this framework to systematically evaluate what kind of regional-scale connections we can (and cannot) make using current OCO-2 observations. We focus on a single year (i.e., 2016) as an initial case study – to explore the applicability of the geostatistical approach to large satellite-based inverse problems. We first describe the implementation of the GIM for OCO-2 observations; we then evaluate and discuss the results of this approach using the 2016 exploratory case study.

## 2 Data and Methods

### 2.1 Approach overview

We design a framework that couples the GIM to a global adjoint model (version v35n of the GEOS-Chem adjoint, Henze et al., 2007) and explore the applicability of the geostatistical approach to inverse problems with a large number of flux grid boxes (i.e.,  $1.2 \times 10^6$ ) and a large number of OCO-2 satellite observations (i.e.,  $9 \times 10^4$ ). We use year 2016 as an initial case study, as there is better temporal coverage of good-quality data from OCO-2 throughout the entire year relative to years 2015 and 2017. For example, there are 7 week-long gaps in the OCO-2 data in year 2015 and a 1.5-month gap in the OCO-2 data



in year 2017, whereas there are no such gaps in year 2016. This time period also overlaps with an OCO-2 inverse modeling  
90 inter-comparison (MIP) study, enabling direct comparison with those results (Crowell et al., 2019). We specifically estimate  
CO<sub>2</sub> fluxes for September 1, 2015 to December 31, 2016 but discard the first four months as a spin-up time period. We also  
offer up a wide range of environmental drivers and allow the GIM to select a subset that best predicts spatiotemporal patterns  
in CO<sub>2</sub> fluxes at the model grid scale, described in detail below (Sects. 2.2-2.4).

## 2.2 OCO-2 satellite observations

95 We utilize 10-s average XCO<sub>2</sub> generated from version 9 of the satellite observations for the period from September 1, 2015  
through the end of year 2016 (e.g., Chevallier et al., 2019). We use both land nadir- and land glint-mode retrievals in the inverse  
model. Recent retrieval updates have eliminated biases that previously existed between land nadir and land glint observations  
(O'Dell et al., 2018). Moreover, Miller and Michalak (2020) evaluated the impact of these updated OCO-2 retrievals on the  
terrestrial CO<sub>2</sub> flux constraint in different regions of the globe; the authors found that the inclusion of both land nadir and land  
100 glint retrievals yielded a stronger constraint on CO<sub>2</sub> fluxes relative to using only a single observation type.

## 2.3 Geostatistical inverse model

A GIM does not require an emission inventory or a bottom-up model as an initial guess of fluxes; instead, a GIM can leverage  
a wide range of environmental driver datasets to help predict spatial and temporal patterns in the CO<sub>2</sub> fluxes (e.g., Gourdji et  
al., 2008, 2012; Shiga et al., 2018). We further pair the GIM with a statistical approach known as model selection to objectively  
105 determine which set of drivers can best reproduce CO<sub>2</sub> observations from OCO-2. This setup makes it feasible to both estimate  
CO<sub>2</sub> fluxes and to explicitly quantify the relationships between the fluxes and the underlying environmental drivers. The fluxes,  
as estimated by the GIM, consist of two components. First, the GIM will scale the environmental drivers to match patterns in  
the atmospheric observations, and this component of the flux estimate is referred to as the ‘deterministic model’. Second, the  
GIM will model space-time patterns in the CO<sub>2</sub> fluxes that are implied by the atmospheric observations but not explained by  
110 any environmental drivers, and this component of the fluxes is referred to as the ‘stochastic component’. The best flux estimate  
is a sum of the deterministic model and the stochastic component:

$$s = \mathbf{X}\beta + \zeta \quad (1)$$

where  $s$  are  $m \times 1$  unknown fluxes,  $\mathbf{X}$  is a  $m \times p$  matrix of environmental drivers (see Sect. 2.4),  $\beta$  are  $p \times 1$  unknown scaling  
factors or drift coefficients. These coefficients quantify the relationships between each of the  $p$  environmental drivers (i.e.,  
115 each column of  $\mathbf{X}$ ) and the estimated CO<sub>2</sub> fluxes. The product of  $\mathbf{X}$  and  $\beta$  is the deterministic model ( $\mathbf{X}\beta$ ). The stochastic  
component ( $\zeta$ ) is zero-mean with a pre-specified spatial and/or temporal correlation structure; it describes spatial and temporal  
patterns in the fluxes that are not captured by the deterministic model. For the setup here, the drift coefficient ( $\beta$ ) associated  
with each environmental driver is constant in space and time, while the stochastic component ( $\zeta$ ) varies at the model grid scale.



We estimate both the fluxes ( $s$ ) and the drift coefficients ( $\beta$ ) by minimizing the GIM cost function (e.g., Kitanidis and  
120 Vomvoris, 1983; Kitanidis, 1995; Michalak et al., 2004):

$$L_{s,\beta} = \frac{1}{2}(z - h(s))^T \mathbf{R}^{-1}(z - h(s)) + \frac{1}{2}(s - \mathbf{X}\beta)^T \mathbf{Q}^{-1}(s - \mathbf{X}\beta) \quad (2)$$

The cost function includes two components: the first component indicates that the fluxes ( $s$ ), when run through an atmospheric  
model,  $h(s)$ , should match the observations ( $z$ ) to within a specific error tolerance ( $z - h(s)$ ) that is prescribed by the covariance  
matrix  $\mathbf{R}$  ( $n \times n$ ).  $\mathbf{R}$  describes model-data mismatch errors, including errors from the atmospheric transport model and the  
125 OCO-2 retrievals, among other errors. The second component of Eq. 2 stipulates that the structure of the stochastic component  
( $s - \mathbf{X}\beta$ ) is described by the covariance matrix  $\mathbf{Q}$  ( $m \times m$ ).  $\mathbf{Q}$ , like  $\mathbf{R}$ , must be defined by the modeler before estimating the  
fluxes; it represents the variances and spatiotemporal covariances of the stochastic component. We estimate  $\mathbf{Q}$  using a statistical  
approach known as Restricted Maximum Likelihood (RML; e.g., Kitanidis, 1997; Gourdjji et al., 2012; Miller et al., 2016).  $\mathbf{Q}$   
includes both diagonal and off-diagonal elements; the latter decay with the separation time and distance between two model  
130 grid boxes. We construct  $\mathbf{R}$  as a diagonal matrix with constant elements on the diagonal. The Supplement Sect. S1 provides a  
detailed explanation of the approach used here to estimate the covariance matrix parameters.

After estimating the covariance matrix parameters, we then estimate the CO<sub>2</sub> fluxes by iteratively minimizing Eq. 2 using  
the Limited-memory Broyden-Fletcher-Goldfarb-Shanno algorithm (L-BFGS, Liu and Nocedal, 1989). We use this approach  
to simultaneously estimate both  $s$  and  $\beta$ . Miller et al (2019) describe this iterative approach to minimize Eq. 2 in detail.

## 135 2.4 Auxiliary environmental drivers

We consider a wide range of environmental drivers ( $\mathbf{X}$ ). These are meteorological variables primarily related to heat, water, and  
radiation, available from NASA's Modern-Era Retrospective Analysis for Research and Applications, Version 2 (MERRA-2,  
Rienecker et al., 2011). Specifically, we consider daily 2-m air temperature, daily precipitation, 30-day average precipitation,  
photosynthetically active radiation (PAR), surface downwelling shortwave radiation, soil temperature at 10-cm depth, soil  
140 moisture at 10-cm depth, specific humidity, and relative humidity. We also include a non-linear function of 2-m air temperature  
as an environmental driver (refer to hereafter as scaled temperature). This function is from the Vegetation Photosynthesis  
and Respiration Model (VPRM, Mahadevan et al., 2008) and describes the non-linear relationship between temperature and  
photosynthesis (e.g., Raich et al. 1991, see the Supplement Sect. S2).

Note that we do not include any remote sensing indices (e.g., solar-induced chlorophyll fluorescence (SIF) or leaf area index  
145 (LAI)) in the present study. Rather, the focus of this study is to explore environmental drivers of CO<sub>2</sub> fluxes, not remote sensing  
proxies for CO<sub>2</sub> fluxes.

We group the globe into seven biome-based regions and allow the GIM to use different environmental drivers in different  
biomes. Miller and Michalak (2020) found that current OCO-2 retrievals can be used to constrain terrestrial CO<sub>2</sub> fluxes for  
regions of this size. The seven-biome map (Fig. 1) is derived from the biomes in Olson et al (2001), aggregated to form larger  
150 regions. As a result of this setup, each column of  $\mathbf{X}$  includes a single environmental driver for a single biome. Therefore, each



environmental driver is represented by a total of seven columns in  $\mathbf{X}$ . Within each column, all elements are zeros except for elements that correspond to a single biome.

We also include several constant columns of ones in  $\mathbf{X}$ . These columns are analogous to the intercept in a linear regression. Existing GIM studies always include one or more constant columns within  $\mathbf{X}$  (e.g., Gourdj et al. 2008; Gourdj et al., 2012; 155 Miller et al., 2018). In this study, we specifically use a total of seven constant columns, one for each biome. We also include a constant column for the ocean.

We further consider non-biospheric fluxes in the  $\mathbf{X}$  matrix, including fossil fuel emissions from the Open-source Data Inventory for Anthropogenic  $\text{CO}_2$  monthly fossil fuel emissions (ODIAC2016, Oda et al., 2018), climatological ocean fluxes from Takahashi et al. (2016), and biomass burning fluxes from the Global Fire Emissions Database (GFED) version 4.1 (Randerson 160 et al., 2018). We only allocate a single column of  $\mathbf{X}$  for fossil fuel, biomass burning, and ocean fluxes, respectively, because these fluxes are not the focus of this study.

In total, we consider a total of 81 columns for the  $\mathbf{X}$  matrix: 8 constant columns of ones, 70 columns associated with environmental drivers, and 3 columns associated with anthropogenic, ocean, and biomass burning fluxes.

## 2.5 Model selection

165 We utilize a model selection framework to evaluate which subset of the environmental drivers (i.e., columns of  $\mathbf{X}$ ) best describe variations in  $\text{CO}_2$  fluxes as inferred from the OCO-2 observations. The inclusion of additional environmental drivers or columns in  $\mathbf{X}$  will always improve the model-data fit, but the inclusion of too many variables in  $\mathbf{X}$  can yield an overfit of the OCO-2 observations or can yield unrealistic drift coefficients ( $\beta$ ) (e.g., Zucchini, 2000). Instead of including all environmental drivers in  $\mathbf{X}$ , we use model selection to decide which set of environmental drivers to include in  $\mathbf{X}$ . In this study, we implement a type 170 of model selection known as the Bayesian Information Criterion (BIC; Schwarz, 1978), which has been extensively used in recent GIM studies (e.g., Gourdj et al., 2012; Miller et al. 2013; Fang and Michalak, 2015). Using the BIC, we score different combinations of environmental drivers that could be included in  $\mathbf{X}$  based on how well each combination reproduces the OCO-2 observations. We calculate these scores using the following equation for the implementation here (Miller et al. 2018; Miller and Michalak, 2020):

$$175 \quad BIC = L + p \ln(n^*) \quad (3)$$

where  $L$  is log likelihood of a particular combination of environmental drivers (i.e., columns of  $\mathbf{X}$ ),  $p$  is the number of environmental drivers in this particular combination, and  $n^*$  is the effective number of independent observations. The first component ( $L$ ) rewards combinations that are a better fit to the observations, whereas the second component in Eq. 3 ( $p \ln(n^*)$ ) penalizes models with a greater number of columns to prevent overfitting. The best combination of environmental drivers for  $\mathbf{X}$  is the 180 combination that receives the lowest score (the Supplement Sect. S3 and Table S2). We implement the BIC using a heuristic branch and bound algorithm (Yadav et al., 2013) to reduce computing time. Miller et al (2018) describes this model selection procedure in greater detail, including the specific setup and equations for the BIC.



## 2.6 Posterior uncertainties

In a GIM, the direct solution to calculate the posterior covariance matrix  $\mathbf{V}_s$  (dimensions  $m \times m$ ) can be computed as (e.g.,  
185 Saibaba and Kitanidis, 2014; Miller et al., 2019):

$$\mathbf{V}_s = \mathbf{V}_1 + \mathbf{V}_2 \mathbf{V}_3 \mathbf{V}_2^T \quad (4)$$

$$\mathbf{V}_1 = (\mathbf{Q}^{-1} + \mathbf{H}^T \mathbf{R}^{-1} \mathbf{H})^{-1} \quad (5)$$

$$\mathbf{V}_2 = \mathbf{V}_1 \mathbf{Q}^{-1} \mathbf{X} \quad (6)$$

$$\mathbf{V}_3 = (\mathbf{X}^T \mathbf{Q}^{-1} \mathbf{X} - (\mathbf{Q}^{-1} \mathbf{X})^T \mathbf{V}_1 \mathbf{Q}^{-1} \mathbf{X})^{-1} \quad (7)$$

190 where the posterior error covariance matrix  $\mathbf{V}_s$  is the sum of  $\mathbf{V}_1$  and  $\mathbf{V}_2 \mathbf{V}_3 \mathbf{V}_2^T$ , and  $\mathbf{H}$  is a  $n \times m$  matrix describing the footprint sensitivity of the observations ( $z$ ) to the fluxes ( $s$ ). Note that  $\mathbf{V}_1$  is the posterior error covariance matrix in a classic Bayesian inverse model (e.g., Rodgers, 2000; Brasseur and Jacob, 2017).  $\mathbf{V}_2 \mathbf{V}_3 \mathbf{V}_2^T$  accounts for the additional uncertainty in the fluxes due to the unknown drift coefficients ( $\beta$ ).

The calculations in Eq. 5 are not computationally feasible for most inverse problems with very large datasets; the matrix sum  
195 in  $\mathbf{V}_1$  is often too large to invert, and we do not explicitly construct an  $\mathbf{H}$  matrix or its transpose  $\mathbf{H}^T$ . Instead, we employ a low-rank approximation of  $\mathbf{V}_1$  that circumvents these problems (e.g., Bousserez and Henze, 2018; Wells et al., 2018). Specifically, we approximate the matrices in  $\mathbf{V}_1$  as a low rank update to  $\mathbf{Q}$  using a limited number of eigenpairs (i.e., eigenvectors and eigenvalues). Miller et al (2019) and the Supplement Sect. S4 describe the uncertainty quantification in greater detail.

## 3 Results and Discussion

### 200 3.1 Connections between CO<sub>2</sub> fluxes and environmental drivers

A small number of environmental drivers can describe most spatiotemporal variability in CO<sub>2</sub> fluxes as estimated in the GIM. In this study, we define spatiotemporal variability as any spatial or temporal patterns in CO<sub>2</sub> fluxes that manifest at the daily, 4° (latitude) × 5° (longitude) resolutions of the GEOS-Chem model during the one-year study period (year 2016). The deterministic model accounts for ~89.6% of the variance in the estimated fluxes (Fig. 2a), and the stochastic component  
205 conversely accounts for only 10.4% of the flux variance (Fig. 2b).

A combination of PAR, daily temperature, and daily precipitation best describe patterns in CO<sub>2</sub> fluxes in most biomes across the globe (Table 1). PAR is an adept predictor of fluxes across mid-to-high latitudes, whereas a combined set of daily air temperature and daily precipitation are better predictors across tropical biomes.

The deterministic model also includes fossil fuel emissions from ODIAC2016 but not biomass burning fluxes from GFED  
210 or ocean fluxes from Takahashi et al., (2016). Fossil fuel emissions from ODIAC2016, when passed through the GEOS-Chem model, help describe enough variability in the OCO-2 observations to be selected using the BIC. By contrast, neither biomass burning fluxes from GFED nor ocean fluxes from Takahashi et al. (2016) help reproduce the OCO-2 observations more than the penalty term in the BIC, and these fluxes are therefore not selected using the BIC. Specifically, biomass burning and



ocean fluxes may not have been selected for several reasons: either those fluxes are small relative to fossil fuel emissions and  
215 biospheric fluxes, the land OCO-2 observations from 2016 are not sensitive to biomass burning and ocean fluxes, and/or the flux  
patterns in GFED and Takahashi et al. (2016) are not consistent with the OCO-2 observations. Instead, biomass burning and  
ocean fluxes are included within the stochastic component of the flux estimate. The Supplement Sect. S6 describes a sensitivity  
analysis using the BIC that provides further explanation why the deterministic model does not include GFED or ocean fluxes  
from Takahashi et al. (2016).

220 Overall, we only select a limited number of environmental drivers (12 out of 70, ~18%) using model selection. Specifically,  
we never select more than 3 environmental drivers in any individual biome (Table 1). This result indicates two likely con-  
clusions. First, a few simple linear relationships may adeptly describe flux variability at the scale and resolution of a global  
gridded atmospheric model, although the underlying leaf- and organism-level processes are admittedly more complex. Indeed,  
previous top-down studies (e.g., Gourdji et al., 2008, 2012; Fang and Michalak, 2015; Shiga et al., 2018) also found that simple  
225 linear relationships can effectively describe broad spatial and temporal patterns in CO<sub>2</sub> flux variability across North America  
and across the globe. Such simple linear relationships allow for a straightforward assessment of the explanatory power of en-  
vironmental drivers, and make it possible to compare these relationships inferred from atmospheric observations against the  
relationships used in TBMs (e.g., Huntzinger et al., 2013; Fang and Michalak, 2015).

Second, additional environmental drivers, when run through an atmospheric transport model and interpolated to the times  
230 and locations of OCO-2 observations, are not sufficiently unique to parse out their differing relationships with CO<sub>2</sub> fluxes.  
Model selection ensures that we only include environmental drivers that contribute unique information to the flux estimate and  
do not overfit the OCO-2 observations. If multiple environmental drivers are highly correlated or colinear, then the inclusion  
of more than one of these drivers will not contribute unique information. As a result, we are unable to quantify a larger number  
of environmental driver relationships using OCO-2. Fig. 3 illustrates an example of air temperature and PAR. In most of the  
235 biomes, there is a weak correlation ( $R < 0.4$ ; left column) between 2-m air temperature and PAR; however, the correlation is  
much stronger ( $R > 0.8$ ; right column) when these environmental drivers are passed through an atmospheric model ( $h(\mathbf{X})$ ). A  
larger number of environmental drivers is not selected due to this high level of correlation or collinearity among the columns in  
 $h(\mathbf{X})$ . This collinearity, not errors in the OCO-2 retrievals or atmospheric model, appears to be a limiting factor in the model  
selection results.

### 240 3.1.1 PAR shows stronger explanatory power than temperature or precipitation in mid-to-high latitudes

PAR is selected for four biomes: temperature forests, temperate grasslands, boreal forests and tropical forests (Table 1). In the  
middle and high latitudes, PAR, rather than temperature or precipitation, appears to be a better proxy for seasonal patterns in  
CO<sub>2</sub> fluxes (Figs. 4a, b and S3a-f). This result reflects the fact that light availability is likely an important factor that drives  
CO<sub>2</sub> flux variability in mid-to-high latitudes (e.g., Fang and Michalak, 2015; Baldocchi et al., 2017). The  $\beta$  values for PAR  
245 indicate a strong to moderate negative correlation with estimated CO<sub>2</sub> fluxes, suggesting that an increase (or decrease) in PAR  
is associated with a decrease (or increase) in NEE, and an increase (or decrease) in carbon uptake; this  $\beta$  value is larger in





boreal and temperate forests relative to grasslands, indicating a stronger relationship between PAR and net biosphere CO<sub>2</sub> fluxes in those biomes (Table 1; Figs. 5a and S3d-f).

Indeed, previous studies also indicate that PAR and similar environmental drivers (e.g., shortwave radiation) are closely associated with CO<sub>2</sub> fluxes. For example, a top-down study of North America (Fang and Michalak, 2015) found that shortwave radiation is more adept than other environmental variables in reproducing spatiotemporal variability of NEE, particularly across the growing season. Moreover, several site-level studies have reached parallel conclusions (e.g., Mueller et al., 2010; Yadav et al., 2010); these studies indicated that PAR is strongly correlated with photosynthesis, consistent with current mechanistic understandings of the light limitation on photosynthesis (e.g., Gough et al., 2007).

### 3.1.2 Drought is likely associated with flux variations across tropical forests

A composite of PAR, scaled temperature, and daily precipitation adeptly describe variability in CO<sub>2</sub> fluxes across tropical forests (Figs. 4c and 4d), as seen through the OCO-2 observations. PAR in tropical forests is usually a function of the presence or absence of clouds (e.g., Baldocchi et al., 2017; Zeri et al., 2014); cloudiness is also associated with rainfall. Therefore, low PAR over tropical forests is likely an indicator of cloud presence and rainfall. A positive  $\beta$  estimated for PAR suggests that a decrease in PAR, indicative of enhanced precipitation, is associated with 380 increased carbon uptake. Furthermore, the negative  $\beta$  value assigned to scaled temperature (the Supplement Sect. S2) implies that an increase in air temperature, which often exceeds optimal temperature over tropical forests, is associated with reduced carbon uptake.

Recent studies (e.g., Jiménez-Muñoz et al., 2016; Liu et al., 2017; Palmer et al., 2019) indicated that tropical droughts associated with the 2015-2016 El Niño events likely resulted in above average carbon release. Indeed, the combination of high values of PAR, high air temperature, and low precipitation may be a manifestation of these drought patterns.

Indeed, multiple lines of evidence indicate that drought is associated with diminished carbon uptake in tropical forests (e.g., Phillips et al., 2009; Brien et al., 2015; Baccini et al., 2017). For example, Gatti et al (2014) suggested that a suppression of photosynthesis during tropical drought may cause a reduction in carbon uptake. Brien et al (2015) added that tropical drought is often associated with higher-than-normal temperature, which may further contribute to reducing gross primary production (GPP) and carbon uptake. Overall, this GIM study supports the conclusion that environmental conditions indicative of drought are associated with net carbon emissions from tropical forests.

### 3.1.3 CO<sub>2</sub> fluxes, as inferred from OCO-2, are closely correlated with temperature and precipitation in tropical grasslands

Temperature and precipitation closely correlate with variability in CO<sub>2</sub> fluxes across tropical grasslands (Figs. S3g and S3j). This result suggests that heat and water availability are likely associated with carbon fluxes across this biome.

A negative  $\beta$  value for precipitation indicates that an increase in precipitation is associated with an increase in carbon uptake, which is in line with current knowledge that water availability facilitates photosynthesis, especially in arid or semi-arid regions. In addition, a negative  $\beta$  value for scaled temperature (the Supplement Sect. S2) indicates that an increase in air temperature is associated with a reduction in carbon uptake. Specifically, high temperatures in the tropics often exceed



280 the optimal temperature for photosynthesis (e.g., Baldocchi et al., 2017), which can suppress GPP (e.g., Doughty and Golden, 2008). Overall, a combined set of air temperature and precipitation adeptly describes CO<sub>2</sub> flux variability in tropical grasslands, rendering it a net source in year 2016.

### 3.2 Estimated biospheric flux totals for different global regions

We estimate a global terrestrial biospheric CO<sub>2</sub> budget of  $-1.73 \pm 0.53$  GtC (Uncertainties listed are the 95% confidence interval. The Supplement Sect. S5 provides detail on the posterior uncertainty estimate for biospheric fluxes.). Among the seven biomes, middle to high latitudes (primarily temperate, boreal and tundra biomes) act as a significant carbon sink; tropical biomes are a net source; desert and shrubland regions play a small, neutral role (Table 2). Note that we subtract flux patterns that map onto fossil fuels ( $X/\beta$ , Fig. 5d) from the posterior flux estimate ( $s$ , Fig. 2c) to obtain an estimate for biospheric fluxes (including terrestrial NEE and biomass burning fluxes). We estimate a  $\beta$  value of  $1.09 \pm 0.05$  (95% confidence interval) for the fossil fuel emissions from ODIAC2016, indicating that the overall global magnitude of ODIAC2016 is consistent with OCO-2 observations. We therefore assume that ODIAC2016 is a reasonable global estimate for fossil fuel emissions.

These flux totals are broadly consistent with a recent MIP of different inverse models that assimilate OCO-2 observations (Crowell et al., 2019). The inverse modeling teams that participated in the MIP employed different transport models, inverse modeling approaches, and prior flux assumptions. The total global terrestrial biospheric flux, averaged across all models, was  $-1.4 \pm 0.7$  GtC for the year of 2016. The MIP fluxes assimilate v7 of land nadir-mode XCO<sub>2</sub> retrievals; unlike this study in which we use v9 of land nadir- and glint-mode retrievals. In spite of this difference, the averaged global flux from the MIP study and the estimate reported here are very similar.

In order to provide an additional comparison with the MIP results, we group the estimated fluxes into TRANSCOM land regions (Gurney et al., 2002). We split the classic TRANSCOM regions at the Equator to avoid regions that encompass parts of both the northern and southern hemisphere, as in Crowell et al (2019). In most of the regions, the fluxes estimated using the GIM are very similar to those reported in the MIP (Fig. 6); however, the fluxes estimated here are significantly different in a limited number of regions (e.g., tropical Australia and northern tropical Africa), a possible reflection of differences between the v9 and v7 OCO-2 retrievals (O'Dell et al., 2018; Miller et al., 2019). For example, we estimate a smaller CO<sub>2</sub> source for northern tropical Africa relative to the MIP study. However, previous studies (e.g., Wang et al., 2019) indicated that existing satellite-based estimates of CO<sub>2</sub> fluxes for this region may be too high. OCO-2 collects far more observations across northern Africa during the dry season than the wet season due to persistent cloudiness in the wet season, and existing studies have postulated that this difference in data availability may be to blame for a high bias in CO<sub>2</sub> fluxes estimated from OCO-2 (Crowell et al. 2019; Wang et al. 2019).

The fluxes estimated here are also broadly consistent with aircraft-based *in situ* CO<sub>2</sub> observations, a topic discussed in the Supplement Sect. S7.



### 3.3 Estimated posterior uncertainties

The posterior uncertainties for individual biomes range from 0.25 to 0.76 GtC yr<sup>-1</sup>. Estimated fluxes for tropical forests have higher uncertainties than any other biome (0.76 GtC yr<sup>-1</sup>), likely a consequence of poor observational coverage due to persistent cloudiness. By contrast, a large number of good-quality OCO-2 retrievals provides robust constraints over temperate  
315 forests, yielding a small posterior uncertainty (0.27 GtC yr<sup>-1</sup>) in the estimated flux.

It is important to note that the posterior uncertainties calculated in most classical Bayesian or geostatistical inverse models account for many but not all possible sources of uncertainty. For example, the posterior uncertainties presented here account for the sparsity of the OCO-2 observations, random observational or atmospheric transport errors, and uncertainties due to uncertain drift coefficients ( $\beta$ ) (e.g., Kitanidis and Vomvoris, 1983; Michalak et al., 2004). However, these calculations do  
320 not fully account for bias-type errors: regional- or continental-scale biases in the OCO-2 observations, biases in modeled atmospheric convection (e.g., Basu et al., 2018; Schuh et al., 2019), or biases in modeled interhemispheric transport, among other possible biases. Most classical Bayesian and geostatistical inverse models assume that the observational or model errors are Gaussian with a mean of zero (e.g., Kitanidis and Vomvoris, 1983; Michalak et al., 2004; Tarantola, 2005), making it  
325 challenging to account for the types of biases listed above. As a result, the posterior uncertainties estimated in this study are typically smaller than the range of flux estimates produced from the recent MIP study (Fig. 6; Crowell et al., 2019).

## 4 Conclusions

In this study, we adapt the geostatistical approach to inverse modeling for global satellite observations of CO<sub>2</sub>, and evaluate the extent to which we can use these observations to make connections between CO<sub>2</sub> fluxes and environmental drivers. We find that

- 330 1. A simple combination of environmental drivers can adeptly describe patterns in CO<sub>2</sub> fluxes across different biomes of the globe, as seen through observations from the OCO-2 satellite;
2. PAR is an adept predictor of fluxes across mid-to-high latitudes, whereas a combination of daily air temperature and daily precipitation shows strong explanatory power across tropical biomes;
- 335 3. A larger number of environmental drivers is not selected because many drivers are correlated or colinear when passed through an atmospheric model and averaged across a total atmospheric column. This high collinearity, not errors in the OCO-2 retrievals or atmospheric model, appears to be a limiting factor in using satellite observations to connect CO<sub>2</sub> fluxes with environmental drivers;
4. We estimate a global terrestrial biospheric budget of  $-1.73 \pm 0.53$  GtC in year 2016, in close agreement with recent inverse modeling studies that use OCO-2 retrievals as observational constraints.



340 *Data availability.* The version 9 of 10-s average OCO-2 retrievals are available at <ftp://ftp.cira.colostate.edu/ftp/BAKER/>; data information of the OCO-2 MIP is available at <https://www.esrl.noaa.gov/gmd/ccgg/OCO2/>; data information of the ObsPack data product is available at <http://www.esrl.noaa.gov/gmd/ccgg/obspack/>.

*Author contributions.* Z.C. and S.M.M. designed the study. Z.C. analyzed the data. Z.C. and S.M.M. wrote the manuscript. All authors reviewed and edited the paper.

345 *Competing interests.* The authors declare they have no competing interests.

*Acknowledgements.* We thank David Baker and Andrew Jacobson for their help with the OCO-2 retrievals and the NASA MIP products. We thank Colm Sweeny and Kathryn McKain for their help with aircraft datasets from the NOAA/ESRL Global Greenhouse Gas Reference Network. We also thank John Miller, Luciana Gatti, Wouter Peters and Manuel Gloor for their help with the aircraft data from the INPE ObsPack data product. Financial support for this research has been provided by NASA ROSES grant no. 80NSSC18K0976. All modeling  
350 and analysis was performed on the NASA Pleiades Supercomputer.



## References

- Baccini, A., Walker, W., Carvalho, L., Farina, M., Sulla-Menashe, D., and Houghton, R. A.: Tropical forests are a net carbon source based on aboveground measurements of gain and loss. *Science*, 358(6360), 230-234. <https://doi.org/10.1126/science.aam5962>, 2017
- Baldocchi, D., Chu, H., and Reichstein, M.: Inter-annual variability of net and gross ecosystem carbon fluxes: A review. *Agricultural and Forest Meteorology*, 249(November 2016), 520–533. <https://doi.org/10.1016/j.agrformet.2017.05.015>, 2018
- 355 Basu, S., Baker, D. F., Chevallier, F., Patra, P. K., Liu, J., and Miller, J. B.: The impact of transport model differences on CO<sub>2</sub> surface flux estimates from OCO-2 retrievals of column average CO<sub>2</sub>. *Atmospheric Chemistry and Physics*, 18(10), 7189-7215, 2018
- Bousserez, N., and Henze, D. K.: Optimal and scalable methods to approximate the solutions of large-scale Bayesian problems: theory and application to atmospheric inversion and data assimilation. *Quarterly Journal of the Royal Meteorological Society*, 144(711), 365-390. DOI:10.1002/qj.3209, 2018
- 360 Brasseur, G. P. and Jacob, D. J.: *Modeling of Atmospheric Chemistry*, chap. 11, Cambridge University Press, Cambridge, <https://doi.org/10.1017/9781316544754>, 2017
- Brienen, R. J. W., Phillips, O. L., Feldpausch, T. R., Gloor, E., Baker, T. R., Lloyd, J., et al.: Long-term decline of the Amazon carbon sink. *Nature*, 519(7543), 344–348. <https://doi.org/10.1038/nature14283>, 2015
- 365 Chatterjee, A., Gierach, M. M., Sutton, A. J., Feely, R. A., Crisp, D., Eldering, A., et al.: Influence of *El Niño* on atmospheric CO<sub>2</sub> over the tropical Pacific Ocean: Findings from NASA's OCO-2 mission. *Science*, 358(6360). <https://doi.org/10.1126/science.aam5776>, 2017
- Commane, R., Lindaas, J., Benmergui, J., Luus, K. A., Chang, R. Y. W., Daube, B. C., et al.: Carbon dioxide sources from Alaska driven by increasing early winter respiration from Arctic tundra. *Proceedings of the National Academy of Sciences of the United States of America*, 114(21), 5361–5366. <https://doi.org/10.1073/pnas.1618567114>, 2017
- 370 Crisp, D.: Measuring atmospheric carbon dioxide from space with the Orbiting Carbon Observatory-2 (OCO-2). *Earth Observing Systems XX*, 9607(September 2015), 960702. <https://doi.org/10.1117/12.2187291>, 2015
- Crowell, S., Baker, D., Schuh, A., Basu, S., Jacobson, A. R., Chevallier, F., Liu, J., Deng, F., Feng, L., McKain, K., Chatterjee, A., Miller, J. B., Stephens, B. B., Eldering, A., Crisp, D., Schimel, D., Nassar, R., O'Dell, C. W., Oda, T., Sweeney, C., Palmer, P. I., and Jones, D. B. A.: The 2015–2016 carbon cycle as seen from OCO-2 and the global *in situ* network, *Atmos. Chem. Phys.*, 19, 9797–9831, <https://doi.org/10.5194/acp-19-9797-2019>, 2019. <https://doi.org/10.5194/acp-2019-87>, 2019
- 375 Chevallier, F.: Comment on “Contrasting carbon cycle responses of the tropical continents to the 2015–2016 *El Niño*”. *Science*, 362(6418), <https://doi.org/10.1126/science.aar5432>, 2018
- Chevallier, F., Palmer, P. I., Feng, L., Boesch, H., O'Dell, C. W., and Bousquet, P.: Toward robust and consistent regional CO<sub>2</sub> flux estimates from *in situ* and spaceborne measurements of atmospheric CO<sub>2</sub>. *Geophysical Research Letters*, 41(3), 1065-1070, 2014
- 380 Chevallier, F., Remaud, M., O'Dell, C. W., Baker, D., Peylin, P., and Cozic, A.: Objective evaluation of surface- and satellite-driven CO<sub>2</sub> atmospheric inversions. *Atmospheric Chemistry and Physics Discussions*, <https://doi.org/10.5194/acp-2019-213>, 2019
- Desai, A. R.: Climatic and phenological controls on coherent regional interannual variability of carbon dioxide flux in a heterogeneous landscape. *Journal of Geophysical Research: Biogeosciences*, 115(G3), 2010
- Eldering, A., Wennberg, P. O., Crisp, D., Schimel, D. S., Gunson, M. R., Chatterjee, A., ... and Frankenberg, C.: The Orbiting Carbon Observatory-2 early science investigations of regional carbon dioxide fluxes. *Science*, 358(6360), eaam5745. DOI: 10.1126/science.aam5745, 2017
- 385



- Eldering, A., Taylor, T. E., O'Dell, C. W., and Pavlick, R.: The OCO-3 mission: Measurement objectives and expected performance based on 1 year of simulated data. *Atmospheric Measurement Techniques*, 12(4), 2341–2370. <https://doi.org/10.5194/amt-12-2341-2019>, 2019
- 390 Fang, Y., and Michalak, A. M.: Atmospheric observations inform CO<sub>2</sub> flux responses to enviroclimatic drivers. *Global Biogeochemical Cycles*, 29(5), 555–566. <https://doi.org/10.1002/2014/GB005034>, 2015
- Gatti, L. V., Gloor, M., Miller, J. B., Doughty, C. E., Malhi, Y., Domingues, L. G., et al.: Drought sensitivity of Amazonian carbon balance revealed by atmospheric measurements. *Nature*, 506(7486), 76–80. <https://doi.org/10.1038/nature12957>, 2014
- Gough, C. M., C. S. Vogel, C. Kazanski, L. Nagel, C. E. Flower, and P. S. Curtis.: Coarse woody debris and the carbon balance of a north temperate forest, *For. Ecol. Manage.*, 244, 60–67, doi:10.1016/j.foreco.2007.03.039, 2007
- 395 Gourdj, Sharon M., Mueller, K. L., Schaefer, K., and Michalak, A. M.: Global monthly averaged CO<sub>2</sub> fluxes recovered using a geostatistical inverse modeling approach: 2. Results including auxiliary environmental data. *Journal of Geophysical Research*, 113(D21), 1–15. <https://doi.org/10.1029/2007jd009733>, 2008
- Gourdj, S. M., Hirsch, A. I., Mueller, K. L., Yadav, V., Andrews, A. E., and Michalak, A. M.: Regional-scale geostatistical inverse modeling of North American CO<sub>2</sub> fluxes: A synthetic data study. *Atmospheric Chemistry and Physics*, 10(13), 6151–6167. <https://doi.org/10.5194/acp-10-6151-2010>, 2010
- 400 Gourdj, S. M., et al.: North American CO<sub>2</sub> exchange: Inter-comparison of modeled estimates with results from a fine-scale atmospheric inversion, *Biogeosciences*, 9(1), 457–475, <https://doi.org/10.5194/bg-9-457-2012>, 2012
- Helfter, C., et al.: Drivers of long-term variability in CO<sub>2</sub> net ecosystem exchange in a temperate peatland. *Biogeosciences* 12 (6), 1799–1811. <https://doi.org/10.5194/bg-12-1799-2015>, 2015
- 405 Houweling, S., Baker, D., Basu, S., Boesch, H., Butz, A., Chevallier, F., et al.: An intercomparison of inverse models for estimating sources and sinks of CO<sub>2</sub> using GOSAT measurements. *Journal of Geophysical Research*, 120(10), 5253–5266. <https://doi.org/10.1002/2014JD022962>, 2015
- Hu, L., Andrews, A. E., Thoning, K. W., Sweeney, C., Miller, J. B., Michalak, A. M., ... and Nehrkorn, T.: Enhanced North American carbon uptake associated with El Niño. *Science advances*, 5(6), eaaw0076, 2019
- 410 Huntzinger, D. N., Schwalm, C., Michalak, A. M., Schaefer, K., King, A. W., Wei, Y., et al.: The North American carbon program multi-scale synthesis and terrestrial model intercomparison project - Part 1: Overview and experimental design. *Geoscientific Model Development*, 6(6), 2121–2133. <https://doi.org/10.5194/gmd-6-2121-2013>, 2013
- Huntzinger, D. N., Michalak, A. M., Schwalm, C., Ciais, P., King, A. W., Fang, Y., et al.: Uncertainty in the response of terrestrial carbon sink to environmental drivers undermines carbon-climate feedback predictions. *Scientific Reports*, 7(1), 1–8. <https://doi.org/10.1038/s41598-017-03818-2>, 2017
- 415 Jimenez-Muñoz, J. C., Mattar, C., Barichivich, J., Santamaría-Artigas, A., Takahashi, K., Malhi, Y., ... and Van Der Schrier, G.: Record-breaking warming and extreme drought in the Amazon rainforest during the course of El Niño 2015–2016. *Scientific reports*, 6, 33130. <https://doi.org/10.1038/srep33130>, 2016
- Kitanidis, P. K., and Vomvoris, E. G.: A geostatistical approach to the inverse problem in groundwater modeling (steady state) and one-dimensional simulations. *Water Resources Research*, 19(3), 677–690, 1983
- 420 Kitanidis, P.: *Introduction to Geostatistics: Applications in Hydrogeology*, Stanford-Cambridge program, Cambridge University Press, Cambridge, 1997



- Kuze, A., Suto, H., Nakajima, M., and Hamazaki, T.: Thermal and near infrared sensor for carbon observation Fourier-transform spectrometer on the Greenhouse Gases Observing Satellite for greenhouse gases monitoring. *Applied Optics*, 48(35), 6716–6733.  
425 <https://doi.org/10.1364/AO.48.006716>, 2009
- Liu, D. C., and Nocedal, J.: On the limited memory BFGS method for large scale optimization. *Mathematical programming*, 45(1-3), 503–528, 1989
- Liu, J., Bowman, K. W., Schimel, D. S., Parazoo, N. C., Jiang, Z., Lee, M., ... and O'Dell, C. W.: Contrasting carbon cycle responses of the tropical continents to the 2015–2016 El Niño. *Science*, 358, 191. [HTTPS://DOI.ORG/ 10.1126/science.aam5690](https://doi.org/10.1126/science.aam5690), 2017
- 430 Mahadevan, P., Wofsy, S. C., Matross, D. M., Xiao, X., Dunn, A. L., Lin, J. C., ... and Gottlieb, E. W.: A satellite-based biosphere parameterization for net ecosystem CO<sub>2</sub> exchange: Vegetation Photosynthesis and Respiration Model (VPRM). *Global Biogeochemical Cycles*, 22(2). <https://doi.org/10.1029/2006GB002735>, 2008
- Ma, S., Baldocchi, D., Wolf, S., Verfaillie, J.: Slow ecosystem responses conditionally regulate annual carbon balance over 15 years in Californian oak-grass savanna. *Agric. Forest Meteorol.* 228, 252–264. <https://doi.org/10.1016/j.agrformet.2016.07.016>, 2016
- 435 Michalak, A. M., Bruhwiler, L., and Tans, P. P.: A geostatistical approach to surface flux estimation of atmospheric trace gases. *Journal of Geophysical Research D: Atmospheres*, 109(14), 1–19. <https://doi.org/10.1029/2003JD004422>, 2004
- Miller, S. M. and Michalak, A. M.: The impact of improved satellite retrievals on estimates of biospheric carbon balance, *Atmos. Chem. Phys.*, 20, 323–331, <https://doi.org/10.5194/acp-20-323-2020>. <https://doi.org/10.5194/acp-20-323-2020>, 2020
- 440 Miller, S. M., Michalak, A. M., Yadav, V., and Tadié, J. M.: Characterizing biospheric carbon balance using CO<sub>2</sub> observations from the OCO-2 satellite. *Atmospheric Chemistry and Physics*, 18(9), 6785–6799. <https://doi.org/10.5194/acp-18-6785-2018>, 2018
- Miller, S. M., Miller, C. E., Commane, R., Chang, R. Y. W., Dinardo, S. J., Henderson, J. M., et al.: A multiyear estimate of methane fluxes in Alaska from CARVE atmospheric observations. *Global Biogeochemical Cycles*, 30(10), 1441–1453. <https://doi.org/10.1002/2016GB005419>, 2016
- 445 Miller, S. M., Saibaba, A. K., Trudeau, M. E., and Andrews, A. E.: Geostatistical inverse modeling with very large datasets: an example from the OCO-2 satellite. *Geoscientific Model Development*, <https://doi.org/10.5194/gmd-2019-185>, 2019
- Miller, S. M., Wofsy, S. C., Michalak, A. M., Kort, E. A., Andrews, A. E., Biraud, S. C., ... and Miller, B. R.: Anthropogenic emissions of methane in the United States. *Proceedings of the National Academy of Sciences*, 110(50), 20018–20022. <https://doi.org/10.1073/pnas.1314392110>, 2013
- 450 Mueller, K. L., Yadav, V., Curtis, P. S., Vogel, C., and Michalak, A. M.: Attributing the variability of eddy-covariance CO<sub>2</sub> flux measurements across temporal scales using geostatistical regression for a mixed northern hardwood forest. *Global Biogeochemical Cycles*, 24(3). <https://doi.org/10.1029/2009GB003642>, 2010
- Nassar, R., Hill, T. G., McLinden, C. A., Wunch, D., Jones, D. B. A., and Crisp, D.: Quantifying CO<sub>2</sub> Emissions From Individual Power Plants From Space. *Geophysical Research Letters*, 44(19), 10,045–10,053. <https://doi.org/10.1002/2017GL074702>, 2017
- 455 Nakajima, M., Kuze, A., and Suto, H.: The current status of GOSAT and the concept of GOSAT-2. In *Sensors, Systems, and Next-Generation Satellites XVI* (Vol. 8533, p. 853306). International Society for Optics and Photonics. <https://doi.org/10.1117/12.974954>, 2012
- Niu, S., Fu, Z., Luo, Y., Stoy, P. C., Keenan, T. F., Poulter, B., ... and Han, J.: Interannual variability of ecosystem carbon exchange: From observation to prediction. *Global ecology and biogeography*, 26(11), 1225–1237, 2017
- O'Dell, C. W., Eldering, A., Wennberg, P. O., Crisp, D., Gunson, M. R., Fisher, B., et al.: Improved retrievals of carbon dioxide from Orbiting Carbon Observatory-2 with the version 8 ACOS algorithm. *Atmospheric Measurement Techniques*, 11(12), 6539–6576.  
460 <https://doi.org/10.5194/amt-11-6539-2018>, 2018



- Oliphant, A., C. Susan, B. Grimmond, H. P. Schmid, and C. A. Wayson: Local-scale heterogeneity of photosynthetically active radiation (PAR), absorbed PAR and net radiation as a function of topography, sky conditions and leaf area index, *Remote Sens. Environ.*, 103(3), 324–337, doi:10.1016/j.rse.2005.09.021, 2006
- Olson, D. M., Dinerstein, E., Wikramanayake, E. D., Burgess, N. D., Powell, G. V. N., Underwood, E. C., et al.: Terrestrial Ecoregions of the World: A New Map of Life on Earth. *BioScience*, 51(11), 933. [https://doi.org/10.1641/0006-3568\(2001\)051\[0933:teotwa\]2.0.co;2](https://doi.org/10.1641/0006-3568(2001)051[0933:teotwa]2.0.co;2), 2006
- 465 Palmer, P. I., Feng, L., Baker, D., Chevallier, F., Bösch, H., and Somkuti, P.: Net carbon emissions from African biosphere dominate pan-tropical atmospheric CO<sub>2</sub> signal. *Nature Communications*, 10(1), 3344. <https://doi.org/10.1038/s41467-019-11097-w>, 2019
- Peters, W., Jacobson, A. R., Sweeney, C., Andrews, A. E., Conway, T. J., Masarie, K., et al.: An atmospheric perspective on North American carbon dioxide exchange: CarbonTracker. *Proceedings of the National Academy of Sciences of the United States of America*, 104(48), 18925–18930. <https://doi.org/10.1073/pnas.0708986104>, 2007
- 470 Peylin, P., Law, R. M., Gurney, K. R., Chevallier, F., Jacobson, A. R., Maki, T., et al.: Global atmospheric carbon budget: Results from an ensemble of atmospheric CO<sub>2</sub> inversions. *Biogeosciences*, 10(10), 6699–6720. <https://doi.org/10.5194/bg-10-6699-2013>, 2013
- Philip, S., Johnson, M. S., Potter, C., Genovesse, V., Baker, D. F., Haynes, K. D., Henze, D. K., Liu, J., and Poulter, B.: Prior biosphere model impact on global terrestrial CO<sub>2</sub> fluxes estimated from OCO-2 retrievals, *Atmos. Chem. Phys.*, 19, 13267–13287, <https://doi.org/10.5194/acp-19-13267-2019>, 2019
- 475 Phillips, O. L., Aragão, L. E., Lewis, S. L., Fisher, J. B., Lloyd, J., López-González, G., ... and Van Der Heijden, G.: Drought sensitivity of the Amazon rainforest. *Science*, 323(5919), 1344–1347. <https://doi.org/10.1126/science.1164033>, 2009
- Piao, S., Liu, Z., Wang, T., Peng, S., Ciais, P., Huang, M., ... and Jeong, S. J.: Weakening temperature control on the interannual variations of spring carbon uptake across northern lands. *Nature Climate Change*, 7(5), 359–363, 2017
- 480 Raich, J. W.: Potential net primary productivity in South America: application of a global model. *Ecological Applications*, 1(4), 399–429. <https://doi.org/10.2307/1941899>, 1991
- Randerson, J.T., G.R. van der Werf, L. Giglio, G.J. Collatz, and P.S. Kasibhatla.: Global Fire Emissions Database, Version 4.1 (GFEDv4). ORNL DAAC, Oak Ridge, Tennessee, USA. <https://doi.org/10.3334/ORNLDAAAC/1293>, 2018
- Rodgers, C. D.: *Inverse methods for atmospheric sounding: theory and practice (Vol. 2)*. World scientific, 2000
- 485 Schuh, A. E., Jacobson, A. R., Basu, S., Weir, B., Baker, D., Bowman, K., ... and Denning, S.: Quantifying the impact of atmospheric transport uncertainty on CO<sub>2</sub> surface flux estimates. *Global Biogeochemical Cycles*, 33(4), 484–500. <https://doi.org/10.1029/2018GB006086>, 2019
- Schwarz, G.: Estimating the dimension of a model, *Ann. Stat.*, 6, 461–464, available at: <http://www.jstor.org/stable/2958889>, 1978
- Shiga, Y. P., Michalak, A. M., Fang, Y., Schaefer, K., Andrews, A. E., Huntzinger, D. H., ... and Wei, Y.: Forests dominate the interannual variability of the North American carbon sink. *Environmental Research Letters*, 13(8), 084015. <https://doi.org/10.1088/1748-9326/aad505>, 2018
- 490 Takahashi, T., Sutherland, S., and Kozyr, A.: Global Ocean Surface Water Partial Pressure of CO<sub>2</sub> Database: Measurements Performed During 1957–2015 (Version 2015), ORNL/CDIAC-160, NDP-088(V2015), Oak Ridge National Laboratory, U.S. Department of Energy, Oak Ridge, Tennessee, [http://doi.org/10.3334/CDIAC/OTG.ND.P088\(V2015\)](http://doi.org/10.3334/CDIAC/OTG.ND.P088(V2015)), 2016
- Tarantola, A.: *Inverse problem theory and methods for model parameter estimation (Vol. 89)*. SIAM, 2005
- 495 Wang, X., Piao, S., Ciais, P., Friedlingstein, P., Myneni, R. B., Cox, P., ... and Yang, H.: A two-fold increase of carbon cycle sensitivity to tropical temperature variations. *Nature*, 506(7487), 212–215, 2014
- Wang, H., Jiang, F., Wang, J., Ju, W., and Chen, J. M.: Terrestrial ecosystem carbon flux estimated using GOSAT and OCO-2 XCO<sub>2</sub> retrievals. *Atmospheric Chemistry and Physics*, 19(18), 12067–12082. <https://doi.org/10.5194/acp-19-12067-2019>, 2019





- 500 Wells, K. C., Millet, D. B., Bousserez, N., Henze, D. K., Griffis, T. J., Chaliyakunnel, S., Dlugokencky, E. J., Saikawa, E., Xiang, G., Prinn,  
R. G., O'Doherty, S., Young, D., Weiss, R. F., Dutton, G. S., Elkins, J. W., Krummel, P. B., Langenfelds, R., and Steele, L. P.: Top-down  
constraints on global N<sub>2</sub>O emissions at optimal resolution: application of a new dimension reduction technique, *Atmospheric Chemistry  
and Physics*, 18, 735–756, <https://doi.org/10.5194/acp18-735-2018>, 2018
- Yadav, V., Mueller, K. L., Dragoni, D., and Michalak, A. M.: A geostatistical synthesis study of factors affecting gross primary productivity  
in various ecosystems of North America. *Biogeosciences*, 7(9), 2655–2671. <https://www.biogeosciences.net/7/2655/2010/>, 2010
- 505 Yadav, V., Mueller, K. L., and Michalak, A. M.: A backward elimination discrete optimization algorithm for model selection in spatio-  
temporal regression models. *Environmental Modelling and Software*, 42, 88–98. <https://doi.org/10.1016/j.envsoft.2012.12.009>, 2013
- Yang, D., Liu, Y., Cai, Z., Chen, X., Yao, L., and Lu, D.: First Global Carbon Dioxide Maps Produced from TanSat Measurements. *Advances  
in Atmospheric Sciences*, 35(6), 621–623. <https://doi.org/10.1007/s00376-018-7312-6>, 2018
- Zeri, M., Sá, L. D. A., Manzi, A. O., Araújo, A. C., Aguiar, R. G., Von Randow, C., et al.: Variability of carbon and water fluxes following  
510 climate extremes over a tropical forest in southwestern amazonia. *PLoS ONE*, 9(2). <https://doi.org/10.1371/journal.pone.0088130>, 2014
- Zucchini, W: An introduction to model selection. *Journal of mathematical psychology*, 44(1), 41–61, 2000

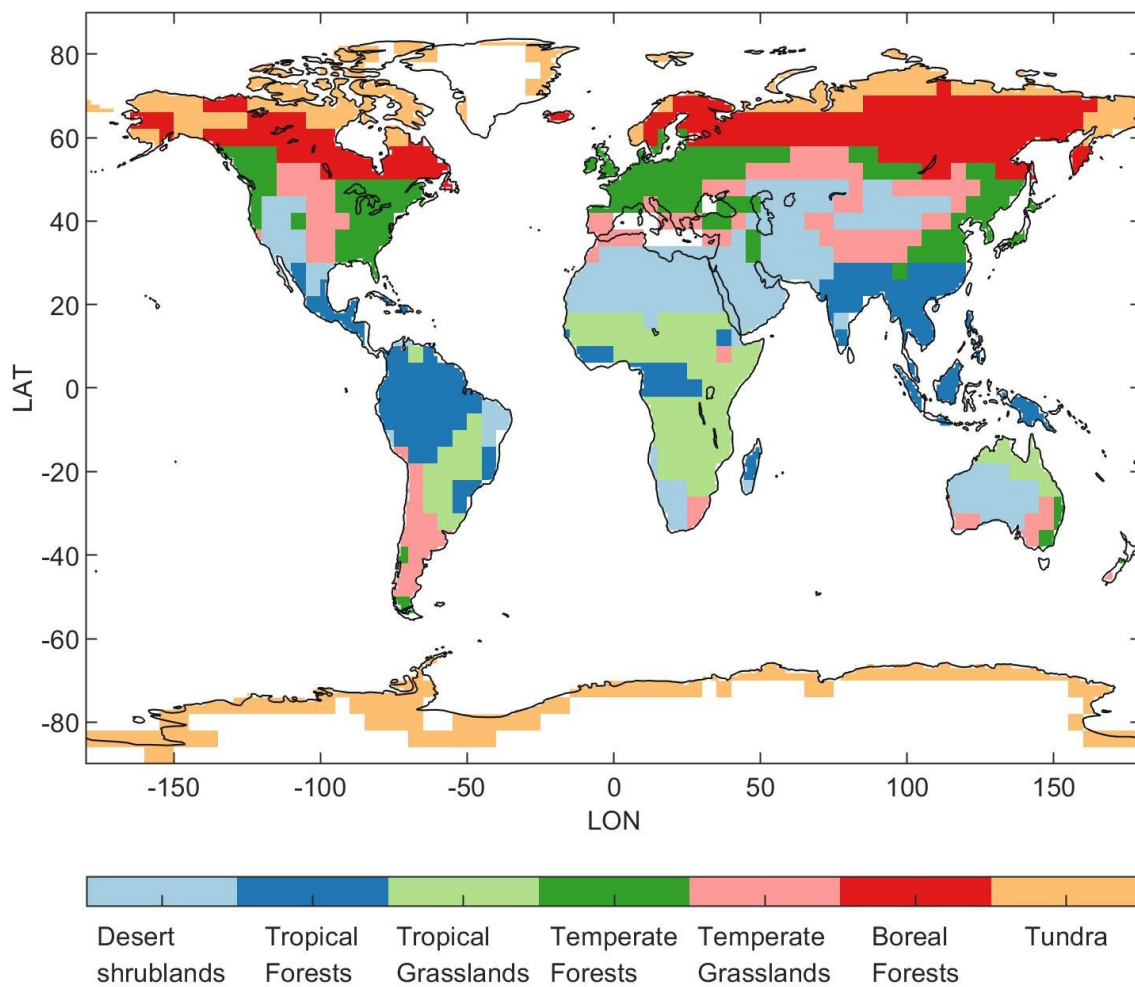


**Figure 1.** The seven biome-based regions aggregated from a world biome map in Olson et al (2001).

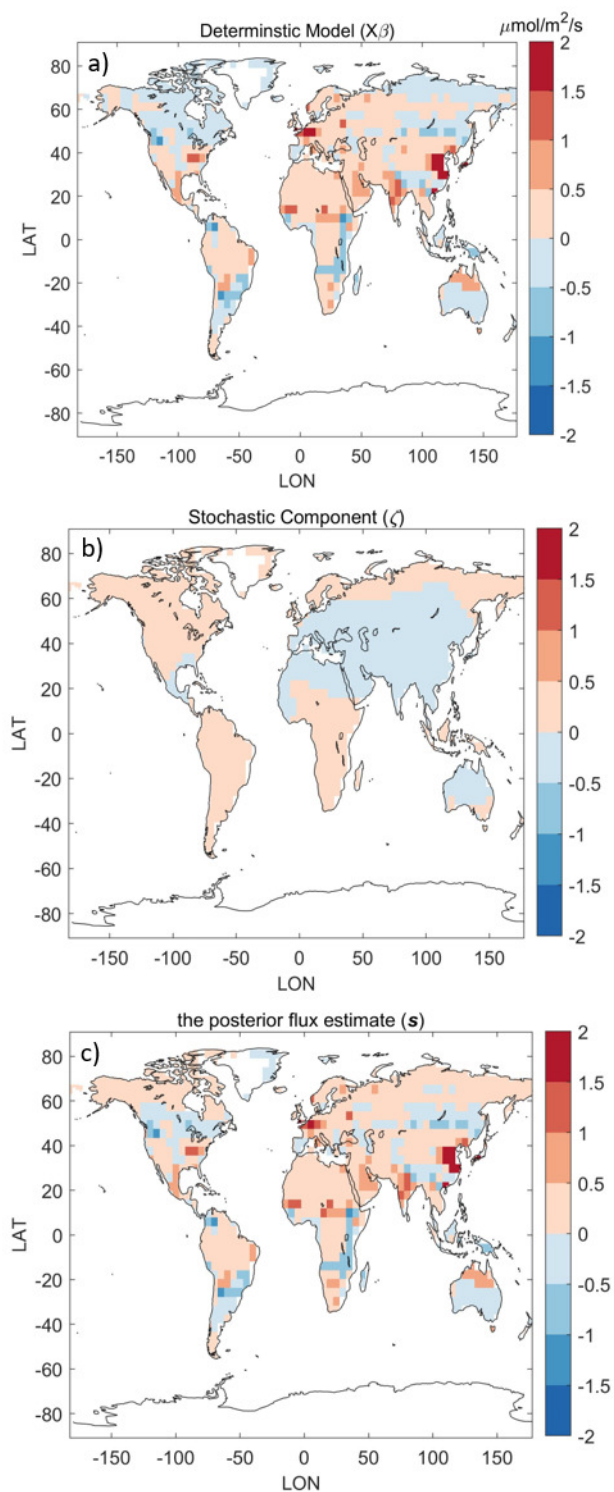


**Figure 2.** Estimated terrestrial fluxes from (a) the deterministic component ( $X\beta$ ) and (b) the stochastic component ( $\zeta$ ). The sum of these two components equals (c) the posterior flux estimates ( $s$ ). Here the posterior flux estimates include contributions from all source types, including flux patterns that map onto fossil fuels from ODIAC2016. **19**

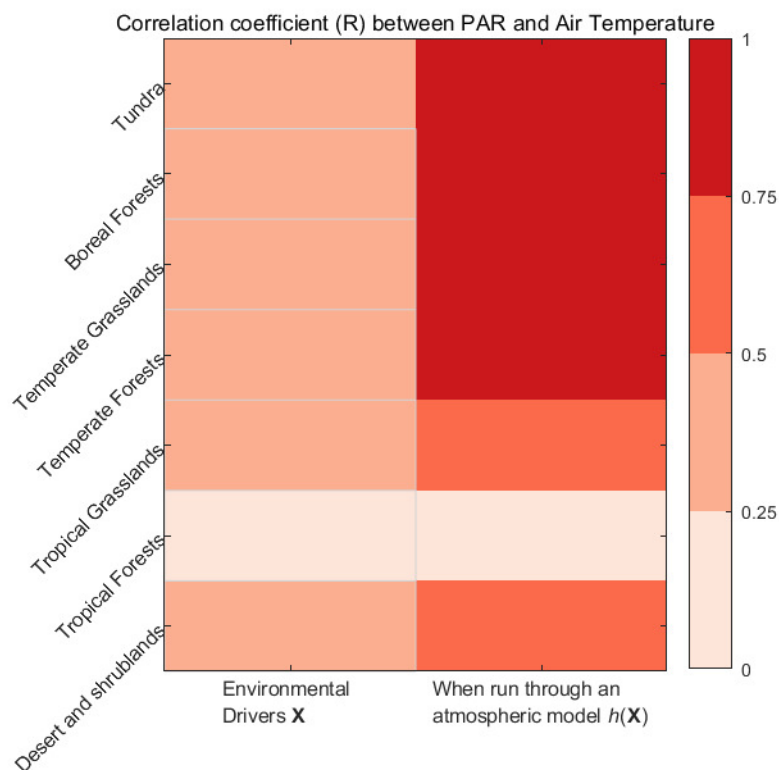


**Figure 3.** . The correlation coefficient (R) between 2-m air temperature and PAR within different global biomes. The left panel shows correlations between air temperature and PAR from MERRA-2, re-gridded to the GEOS-Chem model grid; these environmental drivers are the columns of  $\mathbf{X}$  (Eq. 1). The right panel displays the correlations between these variables after they have been passed through an atmospheric model,  $h(\mathbf{X})$ . The correlation between 2-m air temperature and PAR is weak ( $R < 0.4$ ) in most of the biomes; however, the correlation is much stronger ( $R > 0.8$ ) when these environmental drivers are passed through an atmospheric model. The correlations among other pairs of environmental drivers show similar patterns.

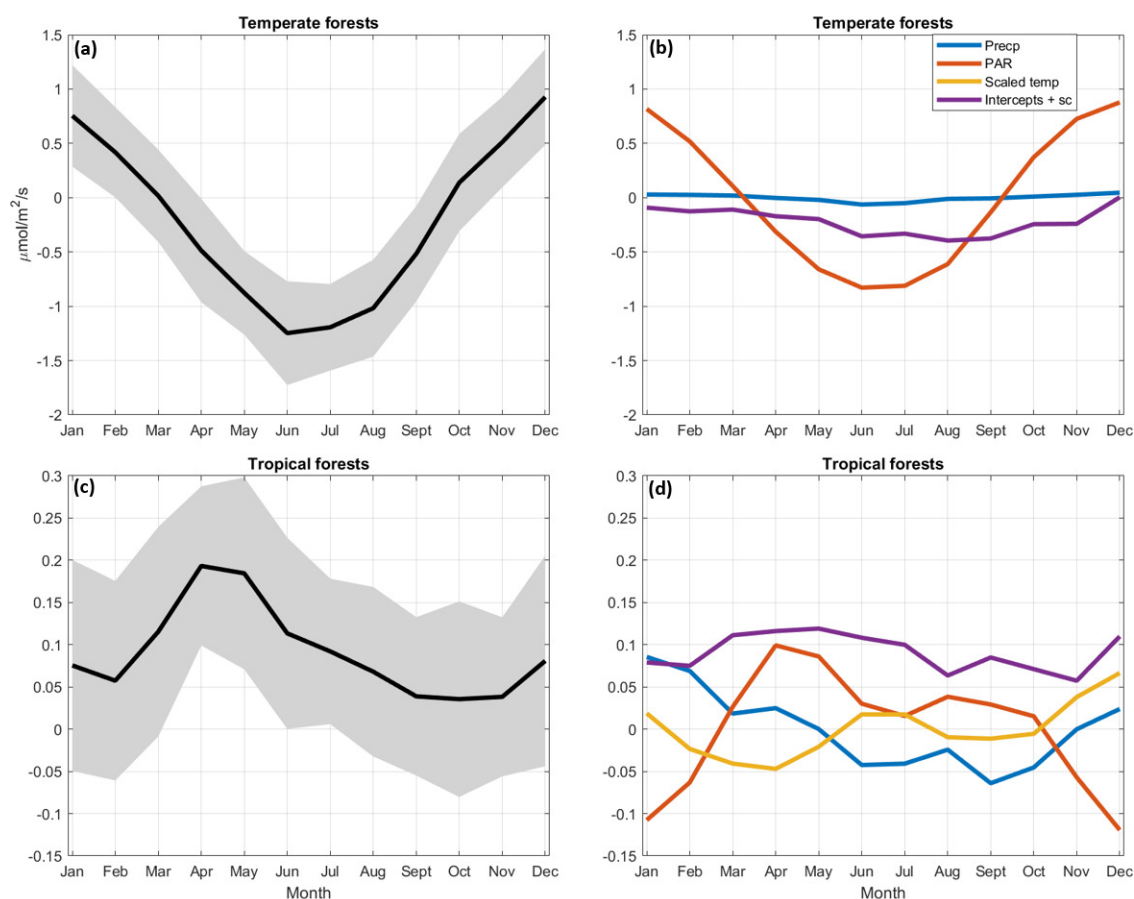


**Figure 4.** Monthly averaged biospheric CO<sub>2</sub> fluxes over (a) temperate forests and (c) tropical forests; and contributions from different environmental drivers ( $\mathbf{X}\beta$ ), the intercept terms and the stochastic component ( $\zeta$ ), respectively, to the flux estimate (b and d). Shaded areas indicate the 95% confidence interval. *Precp*, *Scaled temp*, and *Intercepts + sc* denote daily precipitation, scaled temperature, and combined intercept term and stochastic component, respectively. The example shown here is a prototypical example for two biomes, and Fig. S3 displays the results for all global biomes.

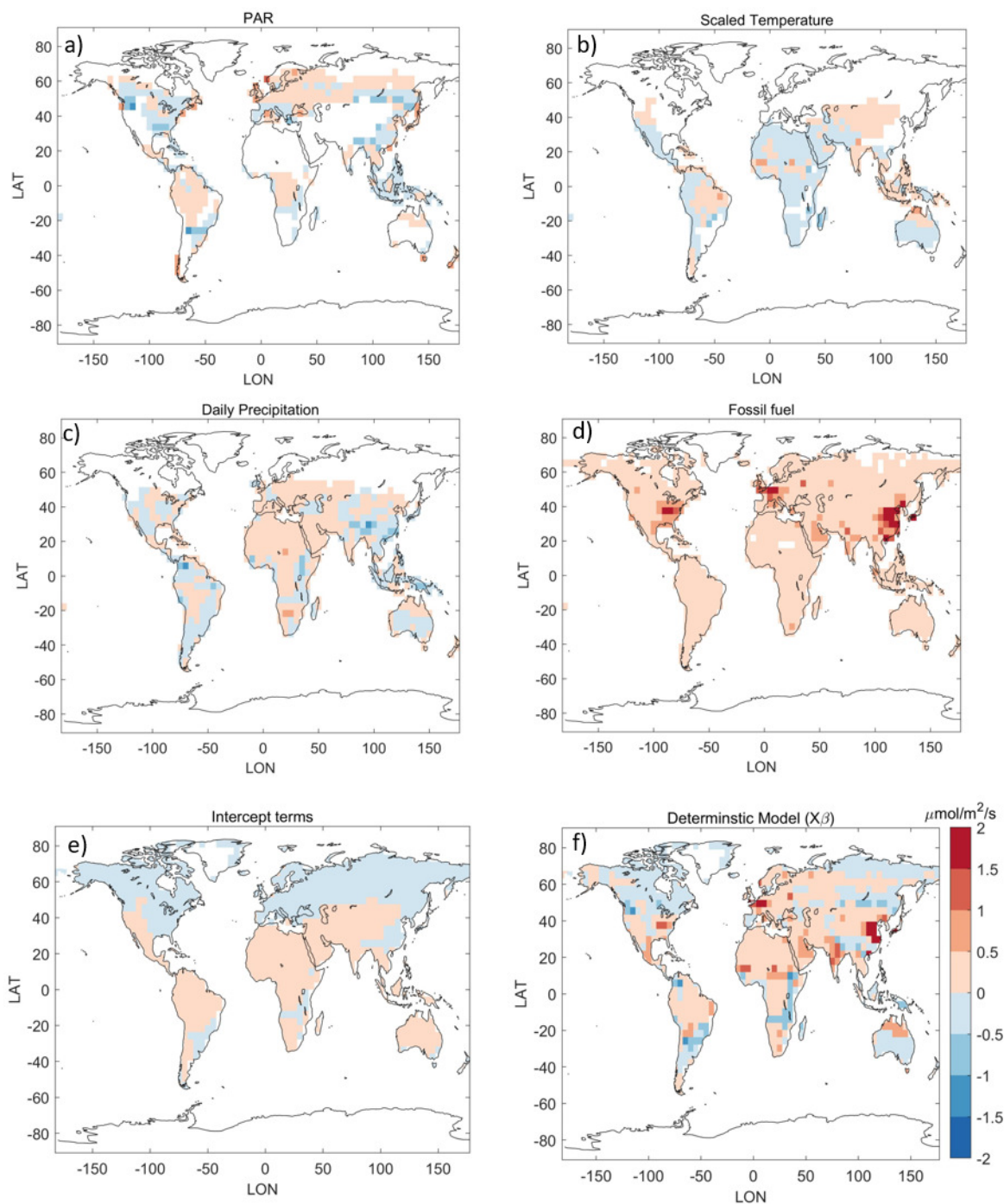


**Figure 5.** The contribution of different environmental drivers ( $X\beta$ ) to estimated CO<sub>2</sub> fluxes from the GIM. The individual panels display the contribution of a) PAR, b) scaled temperature, c) daily precipitation, d) fossil fuel, e) the intercept terms, and f) the full deterministic model ( $X\beta$ ). White colors in panels (a-c) reflect the fact that not all environmental drivers are selected in all biomes.

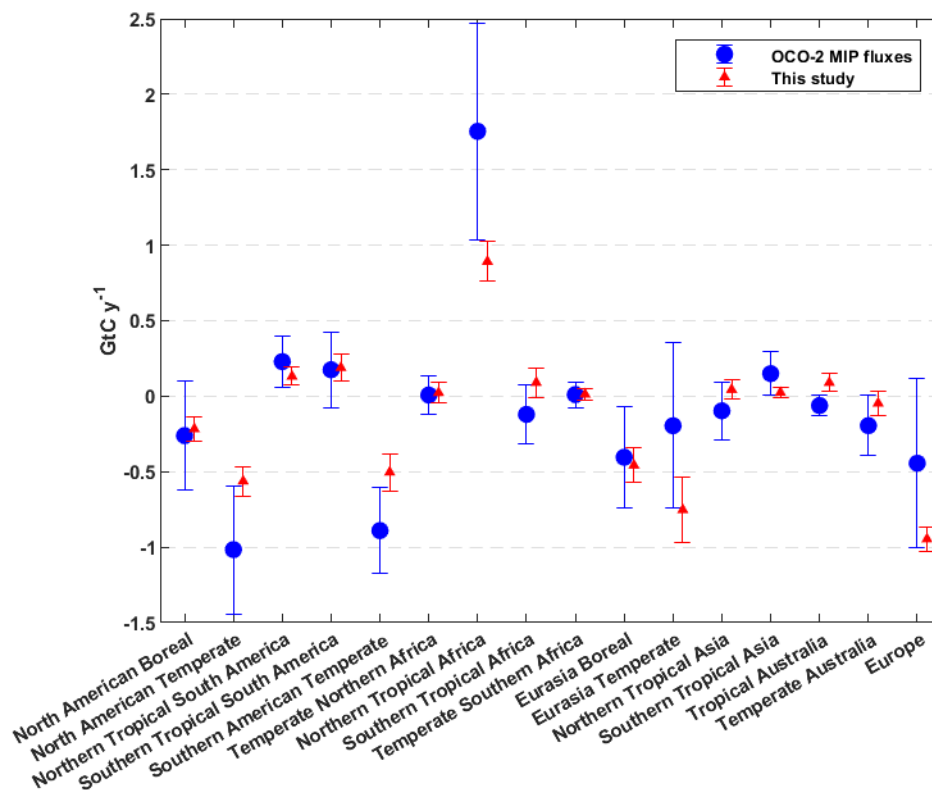


**Figure 6.** Comparison of regional (TRANSCOM-based) biospheric flux estimates in this study (red) and the MIP study (blue).



**Table 1.** Estimated drift coefficients ( $\beta$ ) and associated uncertainties in  $\beta$  for environmental drivers selected using the BIC.

Biomes	Selected environmental drivers	Drift coefficients ( $\beta$ )	Uncertainties in $\beta$ , with 95% confidence interval*
Boreal forests	PAR	-1.20	0.16
Temperate grasslands	Daily precipitation	-0.15	0.05
	PAR	-0.29	0.04
Temperate forests	Daily precipitation	-0.36	0.03
	PAR	-0.81	0.03
Tropical grasslands	Daily precipitation	-0.55	0.06
	Scaled Temperature	-0.35	0.04
Tropical forests	Daily precipitation	-0.23	0.05
	PAR	0.27	0.05
	Scaled Temperature	-0.04	0.02
Desert and shrublands	Daily precipitation	-0.27	0.03
	Scaled Temperature	-0.07	0.01

\*The Supplement Sect. S5 provides detail on the calculations of uncertainties in  $\beta$

**Table 2.** Biospheric CO<sub>2</sub> flux totals estimated for different global biomes.

Biomes	Tundra	Boreal forests	Temperate grasslands	Temperate forests	Tropical grasslands	Tropical forests	Desert/shrublands
Flux budget (Gt C yr <sup>-1</sup> , with 95% confidence interval)	-0.01 ± 0.31	-0.62 ± 0.25	-1.71 ± 0.43	-1.78 ± 0.27	1.21 ± 0.44	1.16 ± 0.76	0.02 ± 0.30